

**ROOM-TEMPERATURE SYNTHESIS OF
BISMUTH OXYBROMIDE-BASED
PHOTOCATALYSTS FOR THE REMOVAL OF
CIPROFLOXACIN FROM AQUEOUS SOLUTION
UNDER VISIBLE LIGHT**

SAIFULLAHI SHEHU IMAM

UNIVERSITI SAINS MALAYSIA

2020

**ROOM-TEMPERATURE SYNTHESIS OF
BISMUTH OXYBROMIDE-BASED
PHOTOCATALYSTS FOR THE REMOVAL OF
CIPROFLOXACIN FROM AQUEOUS SOLUTION
UNDER VISIBLE LIGHT**

by

SAIFULLAHI SHEHU IMAM

**Thesis submitted in fulfilment of the requirements
for the degree of
Doctor of Philosophy**

July 2020

ACKNOWLEDGEMENT

Alhamdulillah, all praises and thanks be to Allah S.W.T for giving me the health, strength and courage to complete this thesis. Countless solat-o-salam on Prophet Muhammad S.A.W for his love and kindness to his Ummah and the entire Humanity.

Besides that, my deep sense of gratitude goes to my supervisor, not only as a supervisor but as a mother, Professor Dr. Rohana Adnan for her continuous guidance, strong motivation, excellent support and inspiration throughout my research work. I consider myself immensely fortunate and privileged to have a supervisor who remained committed to my work at every stage and changed my way of thinking about problems and ways of solving them, without which I would have been unable to complete this work. I shall ever remain grateful to her. May Allah S.W.T bless you more Professor Dr. Rohana Adnan, Ameen summa Ameen.

My special thanks goes to my co-supervisor Dr. Noor Haida Mohd Kaus for her encouragement throughout the research conducted. I would also like to thank my lab members; Dr. Najm, Dr. Amneh, Farah, Shikin, Anis, Rahmah and Ayano for their kindness and moral support. My acknowledgement also goes to respective staff of Universiti Sains Malaysia for their kind assistance and excellent services. I would also like to thank the entire people of Malaysia for their hospitality. The financial support provided by Universiti Sains Malaysia through RUI grant (1001/PKIMIA/811333) and USM Bridging Grant (304/PKIMIA/6316507) is gratefully acknowledged.

Last but not least, my deepest gratitude goes to my family members, especially my late loving mother, for their patience, prayers, understanding and full support.

TABLE OF CONTENTS

ACKNOWLEDGEMENT	ii
TABLE OF CONTENTS	iii
LIST OF TABLES	xi
LIST OF FIGURES	xiii
LIST OF ABBREVIATIONS	xx
ABSTRAK	xxiii
ABSTRACT	xxv
CHAPTER 1 INTRODUCTION	1
1.1 Background.....	1
1.2 Problem Statements	3
1.3 Objectives of the Proposed Study	4
1.4 Scope and Limitations of the Study	4
1.5 Outline of the Thesis	5
CHAPTER 2 LITERATURE REVIEW	6
2.1 Background.....	6
2.2 Advanced Oxidation Processes (AOPs) for Wastewater Treatment	7
2.3 Semiconductor Photocatalysis	7
2.4 Reaction Kinetics	11
2.5 Bismuth-Based Compounds.....	12
2.6 Bismuth Oxybromide (BiOBr)	13
2.7 Synthesis of BiOBr	14
2.7.1 Solvothermal and Hydrothermal Methods	15
2.7.2 Ionothermal Method	16
2.7.3 Microwave-Assisted Method.....	16

2.7.4	Hydrolysis Method	17
2.7.5	Co-precipitation Method	17
2.8	Photocatalytic Enhancement of BiOBr	18
2.8.1	Elemental Doping	18
2.8.2	Coupled Semiconductors	22
2.9	Influence of Operation Parameters on Photocatalytic Degradation Process	28
2.9.1	Catalyst Dosage	28
2.9.2	Initial solution pH	29
2.9.3	Inorganic Ions	30
2.9.4	Scavengers	31
2.10	Immobilization of Photocatalysts	32
2.11	Cellulose Acetate (CA)	36
2.12	Ciprofloxacin	37
2.12.1	Ciprofloxacin Degradation Pathway	42
CHAPTER 3 MATERIALS AND METHODS.....		44
3.1	Materials	44
3.2	Synthesis of BiOBr-Based Composites	45
3.2.1	Synthesis of Pristine BiOBr.....	45
3.2.2	Synthesis of Bi/BiOBr Composites	45
3.2.3	Synthesis of BiOBr/Bi ₂ O ₃ Composites	46
3.2.4	Synthesis of BiOBr/Bi ₂ S ₃ Composites	46
3.2.5	Synthesis of BiOBr/Cellulose Acetate (BCA) Composite Films	47
3.3	Characterizations.....	47
3.3.1	X-Ray Diffraction (XRD).....	47
3.3.2	Field Emission Scanning Electron Microscopy (FESEM).....	48

3.3.3	Attenuated Total Reflection Fourier Transform Infrared (ATR-FTIR)	48
3.3.4	N ₂ Adsorption - Desorption.....	49
3.3.5	UV-Vis Diffuse Reflectance Spectroscopy (DRS).....	49
3.3.6	Photoluminescence Spectroscopy (PL)	50
3.3.7	X-Ray Photoelectron Spectroscopy (XPS).....	51
3.3.8	Thermogravimetric Analysis (TGA)	51
3.3.9	Determination of pH of Point of Zero Charge (pH _{pzc})	51
3.3.10	UV-Visible Spectroscopy	52
3.3.11	Total Organic Carbon (TOC)	52
3.4	Degradation of CIP using Suspended BiOBr-Composites	53
3.4.1	Control Experiments.....	53
3.4.2	Adsorption Kinetic Studies.....	53
3.4.3	Evaluation of Photocatalytic Efficiency	54
3.4.4	Evaluation of Effect of Photocatalyst dosage.....	55
3.4.5	Evaluation of Effect of Photocatalyst Modification.....	55
3.4.6	Evaluation of Effect of Initial Solution pH	55
3.4.7	Evaluation of Effect of Scavengers	56
3.4.8	Evaluation of Effect of Inorganic Ions	56
3.4.9	Recovery Studies	56
3.4.10	Reusability Studies	57
3.5	Degradation of CIP using Immobilized BiOBr Composite Films	57
3.5.1	Evaluation of Effect of Catalyst Loading in Composite Film.....	57
3.5.2	Evaluation of Effect of Composite Film Size.....	57
3.5.3	Evaluation of Effect of Initial Solution pH	58
3.5.4	Evaluation of Effect of Scavengers	58
3.5.5	Reusability Studies	58

CHAPTER 4	RESULTS AND DISCUSSION	
	CHARACTERISATIONS AND CATALYTIC	
	ACTIVITY OF PRISTINE BiOBr AND Bi/BiOBr	
	COMPOSITES	60
4.1	Introduction.....	60
4.2	Characterizations of Pristine BiOBr and Bi/BiOBr Composites	61
4.2.1	X-ray Diffraction (XRD) Analysis.....	61
4.2.2	Field Emission Scanning Electron Microscope (FESEM) Analysis	64
4.2.3	Attenuated Total Reflection-Fourier Transform Infra-red (ATR-FTIR) Analysis	68
4.2.4	X-ray Photoelectron Spectroscopy (XPS) Analysis.....	70
4.2.5	UV-Visible Diffuse Reflectance Spectroscopy (UV-Vis DRS) Analysis	71
4.2.6	Nitrogen Adsorption Analysis (NAA).....	73
4.2.7	Photoluminescence (PL) Analysis.....	75
4.2.8	pH of Point of Zero Charge (pH _{PZC}).....	76
4.3	Activity Studies of Pristine BiOBr and Bi/BiOBr Composites	77
4.3.1	Adsorption Equilibrium Studies	77
4.3.2	Effect of Metallic Bi on the Photocatalytic Activity of BiOBr	78
4.3.3	Photocatalytic Degradation Kinetics	80
4.3.4	Effect of pH on the Photocatalytic Degradation of CIP	83
4.3.5	Effect of Scavengers on the Photocatalytic Degradation of CIP.....	84
4.3.6	Effect of Inorganic Ions on the Photocatalytic Degradation of CIP	86
4.3.7	Mineralization Studies.....	88
4.3.8	Proposed Photocatalytic Mechanism.....	89
4.3.9	Recovery Studies	91
4.3.10	Reusability Studies	92

CHAPTER 5	RESULTS AND DISCUSSION	
	CHARACTERISATIONS AND CATALYTIC	
	ACTIVITY OF PRISTINE BiOBr AND	
	BiOBr/Bi₂O₃ COMPOSITES	94
5.1	Introduction.....	94
5.2	Characterizations of pristine BiOBr and BiOBr/Bi ₂ O ₃ composites.....	95
5.2.1	X-ray Diffraction (XRD) Analysis.....	95
5.2.2	Field Emission Scanning Electron Microscope (FESEM) Analysis.....	97
5.2.3	Attenuated Total Reflection-Fourier Transform Infra-red (ATR-FTIR) Analysis.....	101
5.2.4	X-ray Photoelectron Spectroscopy (XPS) Analysis.....	103
5.2.5	UV-Visible Diffuse Reflectance Spectroscopy (UV-Vis DRS) Analysis.....	104
5.2.6	Nitrogen Adsorption Analysis (NAA).....	106
5.2.7	Photoluminescence Analysis (PL).....	108
5.2.8	pH of Point of Zero Charge (pH _{PZC}).....	109
5.3	Activity Studies of Pristine BiOBr and BiOBr/Bi ₂ O ₃ Composites.....	110
5.3.1	Adsorption Equilibrium Studies.....	110
5.3.2	Effect of Alkali Etching Duration on the Photocatalytic Activity of BiOBr.....	111
5.3.3	Degradation Kinetics.....	114
5.3.4	Effect of pH on the Photocatalytic Degradation of CIP.....	115
5.3.5	Effect of Scavengers on the Photocatalytic Degradation of CIP.....	117
5.3.6	Effect of Inorganic Ions on the Photocatalytic Degradation of CIP.....	118
5.3.7	Mineralization Studies.....	119
5.3.8	Proposed Photocatalytic Mechanism.....	120
5.3.9	Recovery Studies.....	123

5.3.10	Reusability Studies	124
CHAPTER 6 RESULTS AND DISCUSSION		
CHARACTERIZATIONS AND CATALYTIC		
ACTIVITY OF PRISTINE BiOBr AND		
Bi₂S₃/BiOBr COMPOSITES..... 126		
6.1	Introduction.....	126
6.2	Characterizations of Pristine BiOBr and BiOBr/Bi ₂ S ₃ Composites.....	127
6.2.1	X-ray Diffraction (XRD) Analysis.....	127
6.2.2	Field Emission Scanning Electron Microscope (FESEM) Analysis	129
6.2.3	Attenuated Total Reflection-Fourier Transform Infra-red (ATR-FTIR) Analysis	133
6.2.4	X-ray Photoelectron Spectroscopy (XPS) Analysis.....	135
6.2.5	UV-Visible Diffuse Reflectance Spectroscopy (UV-Vis DRS) Analysis	136
6.2.6	Nitrogen Adsorption Analysis (NAA).....	138
6.2.7	Photoluminescence Analysis (PL).....	140
6.2.8	pH of Point of Zero Charge (pH _{PZC}).....	141
6.3	Activity Studies of Pristine BiOBr and BiOBr/Bi ₂ S ₃ Composites	142
6.3.1	Adsorption Equilibrium Studies.....	142
6.3.2	Effect of Sulfidation Duration on the Photocatalytic Activity of BiOBr.....	143
6.3.3	Photocatalytic Degradation Kinetics	146
6.3.4	Effect of pH on the Photocatalytic Activity of BiOBr/Bi ₂ S ₃ -60	148
6.3.5	Effect of Scavengers on the Photocatalytic Activity of BiOBr/Bi ₂ S ₃ -60	149
6.3.6	Effect of Inorganic Ions on the Photocatalytic Activity of BiOBr/Bi ₂ S ₃ -60	150
6.3.7	Mineralization Studies.....	151
6.3.8	Proposed Photocatalytic Mechanism.....	152

6.3.9	Recovery Studies	155
6.3.10	Reusability Studies	156
CHAPTER 7 RESULTS AND DISCUSSION		
CHARACTERISATIONS AND CATALYTIC		
ACTIVITY OF CELLULOSE ACETATE AND		
BiOBr/CELLULOSE ACETATE COMPOSITE		
FILMS		
		158
7.1	Introduction.....	158
7.2	Characterizations of CA and BCA Composite Films	159
7.2.1	X-ray Diffraction (XRD) Analysis	159
7.2.2	Field Emission Scanning Electron Microscope (FESEM) Analysis	161
7.2.3	Attenuated Total Reflection-Fourier Transform Infra-red (ATR-FTIR) Analysis	166
7.2.4	UV-Visible Diffuse Reflectance Spectroscopy (UV-Vis DRS) Analysis	168
7.2.5	Thermogravimetric Analysis (TGA)	169
7.3	Activity Studies of BCA Composite Films.....	171
7.3.1	Effect of BiOBr Loading	171
7.3.2	Effect of Film Size.....	174
7.3.3	Effect of pH	176
7.3.4	Effect of Scavengers	179
7.3.5	Mineralization Studies.....	181
7.3.6	Proposed Photocatalytic Mechanism.....	182
7.3.7	Reusability and Stability Studies.....	183
CHAPTER 8 CONCLUSIONS AND RECOMMENDATIONS		
		187
8.1	Conclusions.....	187
8.2	Recommendations for Future Studies	189

REFERENCES..... 190

APPENDICES

LIST OF PUBLICATIONS AND PRESENTATIONS

LIST OF TABLES

		Page
Table 2.1	Comparative degradation efficiencies of various pristine and doped BiOBr photocatalysts	21
Table 2.2	Comparative degradation efficiencies of various pristine and coupled BiOBr photocatalysts.....	25
Table 2.3	Examples of commonly used scavengers	32
Table 2.4	Photocatalytic degradation efficiencies of various polymer-based hybrid immobilized systems	34
Table 2.5	Comparative CIP degradation by various photocatalysts in the literature	39
Table 3.1	List of chemicals used in the present study, their purity, brand and origin.	44
Table 4.1	Surface area, pore volume and band gap energy of pristine BiOBr and Bi/BiOBr composites.	73
Table 4.2	Equilibrium adsorption capacities, pseudo-first order and pseudo-second order correlation coefficients and rate constants for the photocatalytic degradation of CIP using pristine BiOBr and Bi/BiOBr composites.	82
Table 4.3	Correlation coefficients (R^2) and rate constants (k) of trapping experiment using Bi/BiOBr-20 composite photocatalyst.	86
Table 4.4	Correlation coefficients and rate constants of Bi/BiOBr-20 composite during catalyst recovery test.	92
Table 5.1	Surface area, pore volume and band gap energy of pristine BiOBr and BiOBr/Bi ₂ O ₃ composites photocatalysts.	106
Table 5.2	Equilibrium adsorption capacities, pseudo-first order and pseudo-second order correlation coefficients and rate constants for the photocatalytic degradation of CIP using pristine BiOBr and BiOBr/Bi ₂ O ₃ -60 composites.....	115
Table 5.3	Correlation coefficients (R^2) and rate constants (k) of trapping experiment using BiOBr/Bi ₂ O ₃ -60 composite.....	118
Table 5.4	Correlation coefficients and rate constants of BiOBr/Bi ₂ O ₃ -60 composite during recovery test.....	124

Table 6.1	Surface area, pore volume and band gap energy of pristine BiOBr and BiOBr/Bi ₂ S ₃ composites photocatalysts.....	138
Table 6.2	Equilibrium adsorption capacities, pseudo-first order and pseudo-second order correlation coefficients and rate constants for the photocatalytic degradation of CIP using pristine BiOBr and BiOBr/Bi ₂ S ₃ composites.....	147
Table 6.3	Correlation coefficients and rate constants of trapping experiment using BiOBr/Bi ₂ S ₃ -60 composite photocatalyst.	150
Table 6.4	Correlation coefficients and rate constants of BiOBr/Bi ₂ S ₃ -60 during leaching test.	156
Table 7.1	Equilibrium adsorption capacities, pseudo-first order and pseudo-second order correlation coefficients and rate constants for the photocatalytic degradation of CIP using pristine BiOBr and BCA composite films.	173
Table 7.2	Pseudo-first order correlation coefficients (R^2) and rate constants (k) for the photocatalytic degradation of CIP different sizes of BCA-30 composite film.	176
Table 7.3	Pseudo-first order correlation coefficients (R^2) and rate constants (k) for the photocatalytic degradation of CIP at different pH's, using 3×3 cm ² of BCA-30 composite film.	178
Table 7.4	Pseudo-first order correlation coefficients (R^2) and rate constants (k) for the photocatalytic degradation of CIP in the presence of scavengers, using 3×3 cm ² of BCA-30 composite film.	181

LIST OF FIGURES

	Page
Figure 1.1	Framework of the thesis 5
Figure 2.1	Schematic illustration for the generation of oxidative species in a photocatalytic reaction (Chong <i>et al.</i> , 2010)..... 9
Figure 2.2	Crystal structure of BiOX (X = F, Cl, Br, I) systems (Ganose <i>et al.</i> , 2016). 14
Figure 2.3	Chemical structure of cellulose acetate (Chen <i>et al.</i> , 2015). 36
Figure 2.4	Chemical structure of ciprofloxacin (CIP) (Khoshnamvand <i>et al.</i> , 2018)..... 37
Figure 2.5	Possible pathways of CIP photodegradation (Jia <i>et al.</i> , 2020)..... 43
Figure 3.1	Schematic of the experimental set-up used for photodegradation of CIP..... 54
Figure 4.1	Color change in BiOBr samples with different bismuth loading 61
Figure 4.2	XRD patterns of (a) as-synthesized pristine and Bi/BiOBr composites and (b) enlarged view of diffraction region between 25°- 45°. 62
Figure 4.3	FESEM images of (a, b) pristine BiOBr, (c) Bi/BiOBr-5, (d) Bi/BiOBr-10, (e) Bi/BiOBr-20 and (f) Bi/BiOBr-30..... 65
Figure 4.4	ATR-FTIR spectra of as-synthesized pristine BiOBr and Bi/BiOBr composites..... 69
Figure 4.5	XPS spectra of Bi/BiOBr-20 composite. (a) survey scan (b) Bi 4f (c) O 1s and (d) Br 3d..... 70
Figure 4.6	(a) UV-vis diffuse reflectance spectra and Tauc's plot of $(\alpha h\nu)^{0.5}$ vs. E (eV) for (b) as-synthesized pristine BiOBr, (c) Bi/BiOBr-5, (d) Bi/BiOBr-10, (e) Bi/BiOBr-20, and (f) Bi/BiOBr-30. 72
Figure 4.7	N ₂ adsorption – desorption isotherms and the corresponding pore size distribution (insets) for (a) as-synthesized pristine BiOBr, (b) Bi/BiOBr-5, (c) Bi/BiOBr-10, (d) Bi/BiOBr-20 and (e) Bi/BiOBr-30. 74
Figure 4.8	PL spectra of pristine BiOBr and Bi/BiOBr composites..... 76

Figure 4.9	Point of zero charges of pristine BiOBr and Bi/BiOBr composites.	77
Figure 4.10	(a) Adsorption kinetics curves and (b) equilibrium adsorption capacities of CIP over pristine BiOBr and Bi/BiOBr composites.....	78
Figure 4.11	Variation in absorption vs wavelength for the photocatalytic degradation of CIP as a function of irradiation time in the presence of (a) as-synthesized pristine BiOBr, (b) Bi/BiOBr-5, (c) Bi/BiOBr-10, (d) Bi/BiOBr-20 and (e) Bi/BiOBr-30.	79
Figure 4.12	Percentage of removal versus reaction time for CIP (20 mg/L, pH 7.1 ± 0.05) removal from aqueous solution in-dark and under indoor fluorescent light illumination using 0.1 g of pristine BiOBr and Bi/BiOBr composites.....	80
Figure 4.13	(a) Pseudo-first order kinetic and (b) pseudo-second order kinetic plots for the degradation of CIP using pristine BiOBr and Bi/BiOBr composites under indoor fluorescent light illumination.	81
Figure 4.14	Effect of pH on adsorption and photocatalysis of CIP (20 mg/L) from aqueous solution under indoor fluorescent light illumination by Bi/BiOBr-20.....	83
Figure 4.15	(a) Effect of various scavengers on photocatalytic efficiency and (b) kinetic curves of Bi/BiOBr-20 towards CIP degradation under indoor fluorescent light illumination.....	85
Figure 4.16	Effect of inorganic salts on the degradation of CIP in the presence of Bi/BiOBr-20.....	87
Figure 4.17	TOC removal in the presence of Bi/BiOBr-20.....	88
Figure 4.18	Proposed mechanism for the photocatalytic degradation of CIP over Bi/BiOBr-20 composite under indoor fluorescent light illumination.	89
Figure 4.19	(a) Recovery test exhibited by Bi/BiOBr-20 and (b) the kinetic curves.....	91
Figure 4.20	Recycling performance of photocatalytic degradation of CIP over Bi/BiOBr-20 composite under indoor fluorescent light illumination.	93
Figure 4.21	Comparison of FTIR spectra of Bi/BiOBr-20 composite before and after photocatalytic degradation of CIP (reuse five times).....	93

Figure 5.1	Color change in BiOBr samples with different alkali etching durations	95
Figure 5.2	(a) XRD patterns of as-synthesized pristine BiOBr and BiOBr/Bi ₂ O ₃ composites and (b) enlarged view of diffraction region between 20°- 35°	96
Figure 5.3	FESEM images of (a, b) pristine BiOBr, (c) BiOBr/Bi ₂ O ₃ -10, (d) BiOBr/Bi ₂ O ₃ -30, (e) BiOBr/Bi ₂ O ₃ -60 and (f) BiOBr/Bi ₂ O ₃ -120.....	98
Figure 5.4	ATR-FTIR spectra of as-synthesized pristine BiOBr and BiOBr/Bi ₂ O ₃ composites.....	102
Figure 5.5	XPS spectra of BiOBr/Bi ₂ O ₃ -60 composite. (a) survey scan, (b) Bi 4f, (c) O 1s and (d) Br 3d.	103
Figure 5.6	(a) UV-Vis diffuse reflectance spectra of pristine BiOBr and BiOBr/Bi ₂ O ₃ composites and Tauc's plot of $(\alpha h\nu)^{0.5}$ vs. E (eV) for (b) as-synthesized pristine BiOBr, (c) BiOBr/Bi ₂ O ₃ – 10, (d) BiOBr/Bi ₂ O ₃ – 30, (e) BiOBr/Bi ₂ O ₃ – 60 and (f) BiOBr/Bi ₂ O ₃ – 120.	105
Figure 5.7	N ₂ adsorption – desorption isotherms and the corresponding pore size distribution (insets) for (a) as-synthesized pristine BiOBr, (b) BiOBr/Bi ₂ O ₃ – 10, (c) BiOBr/Bi ₂ O ₃ – 30, (d) BiOBr/Bi ₂ O ₃ – 60 and (f) BiOBr/Bi ₂ O ₃ – 120.....	107
Figure 5.8	PL spectra of pristine BiOBr and BiOBr/Bi ₂ O ₃ composites.....	109
Figure 5.9	Point of zero charges of pristine BiOBr and BiOBr/Bi ₂ O ₃ composites.....	110
Figure 5.10	(a) Adsorption kinetics curves and (b) equilibrium adsorption capacities of CIP over pristine BiOBr and BiOBr/Bi ₂ O ₃ composites.....	111
Figure 5.11	Variation in absorption vs wavelength for the photocatalytic degradation of CIP as a function of irradiation time in the presence of (a) as-synthesized pristine BiOBr, (b) BiOBr/Bi ₂ O ₃ -10, (c) BiOBr/Bi ₂ O ₃ -30, (d) BiOBr/Bi ₂ O ₃ -60 and (e) BiOBr/Bi ₂ O ₃ -120.	112
Figure 5.12	Percentage of removal versus reaction time for CIP (20 mg/L, pH 7.1 ± 0.05) removal from aqueous solution in-dark and under indoor fluorescent light illumination using 0.1 g of pristine BiOBr and BiOBr/Bi ₂ O ₃ composites.	113

Figure 5.13	(a) Pseudo-first order kinetic and (b) pseudo-second order kinetic plots for the degradation of CIP using pristine BiOBr and BiOBr/Bi ₂ O ₃ composites under indoor fluorescent light illumination.	114
Figure 5.14	Effect of pH on adsorption and photocatalysis of CIP from aqueous solution under indoor fluorescent light illumination by BiOBr/Bi ₂ O ₃ -60 composite.....	116
Figure 5.15	Effect of various scavengers on photocatalytic efficiency (a) kinetic curves (b) of BiOBr/Bi ₂ O ₃ -60 composite towards CIP degradation under indoor fluorescent light illumination.....	117
Figure 5.16	Effect of inorganic salts on the degradation of CIP in the presence by BiOBr/Bi ₂ O ₃ -60 composite under indoor fluorescent light illumination.	119
Figure 5.17	TOC removal in the presence of BiOBr/Bi ₂ O ₃ -60 composite.....	120
Figure 5.18	Proposed mechanism for the photocatalytic degradation of CIP over BiOBr/Bi ₂ O ₃ -60 composite under indoor fluorescent light illumination.	121
Figure 5.19	(a) Recovery test exhibited by BiOBr/Bi ₂ O ₃ -60 and (b) kinetic curves.....	123
Figure 5.20	Recycling performance of photocatalytic degradation of CIP over BiOBr/Bi ₂ O ₃ -60 composite under indoor fluorescent light illumination.	125
Figure 5.21	Comparison of FTIR spectra of BiOBr/Bi ₂ O ₃ -60 composite before and after photocatalytic degradation of CIP (reuse five times).....	125
Figure 6.1	Color change in the samples after different sulfidation durations	127
Figure 6.2	XRD patterns of as-synthesized pristine and BiOBr/Bi ₂ S ₃ composites	128
Figure 6.3	FESEM images of (a, b) pristine BiOBr, (c) BiOBr/Bi ₂ S ₃ -10, (d) BiOBr/Bi ₂ S ₃ -30, (e) BiOBr/Bi ₂ S ₃ -60 and (f) BiOBr/Bi ₂ S ₃ -120.	130
Figure 6.4	ATR-FTIR spectra of as-synthesized pristine BiOBr and BiOBr/Bi ₂ S ₃ composites.....	134
Figure 6.5	XPS spectra of BiOBr/Bi ₂ S ₃ -60 composite. (a) survey scan, (b) Bi 4f, (c) O 1s, (d) Br 3d and (e) S 2p.	135

Figure 6.6	(a) UV-vis diffuse reflectance spectra and Tauc's plot of $(\alpha h\nu)^{0.5}$ vs. E (eV) for as-synthesized (b) pristine BiOBr, (c) BiOBr/Bi ₂ S ₃ -10, (d) BiOBr/Bi ₂ S ₃ -30, (e) BiOBr/Bi ₂ S ₃ -60 and (f) BiOBr/Bi ₂ S ₃ -120.....	137
Figure 6.7	N ₂ adsorption – desorption isotherms and the corresponding pore size distribution (insets) for as-synthesized (a) pristine BiOBr, (b) BiOBr/Bi ₂ S ₃ -10, (c) BiOBr/Bi ₂ S ₃ -30, (d) BiOBr/Bi ₂ S ₃ -60 and (e) BiOBr/Bi ₂ S ₃ -120.	139
Figure 6.8	PL spectra of pristine BiOBr and BiOBr/Bi ₂ S ₃ composites.....	141
Figure 6.9	Point of zero charges of pristine BiOBr and BiOBr/Bi ₂ S ₃ composites.	142
Figure 6.10	(a) Adsorption kinetics curve and (b) equilibrium adsorption capacities of CIP over pristine BiOBr and BiOBr/Bi ₂ S ₃ composites.....	143
Figure 6.11	Variation in absorption vs wavelength for the photocatalytic degradation of CIP as a function of irradiation time in the presence of as-synthesized pristine (a) BiOBr, (b) BiOBr/Bi ₂ S ₃ -10, (c) BiOBr/Bi ₂ S ₃ -30, (d) BiOBr/Bi ₂ S ₃ -60 and (e) BiOBr/Bi ₂ S ₃ -120.	144
Figure 6.12	Percentage of removal versus reaction time for CIP (20 mg/L, pH 7.1 ± 0.05) removal from aqueous solution in-dark and under indoor fluorescent light illumination using 0.1 g of pristine BiOBr and BiOBr/Bi ₂ S ₃ composites.....	145
Figure 6.13	(a) Pseudo-first order kinetic and (b) pseudo-second order kinetic plot for the degradation of CIP using pristine BiOBr and BiOBr/Bi ₂ S ₃ composites under indoor fluorescent light illumination.....	146
Figure 6.14	Effect of pH on adsorption and photocatalysis of CIP from aqueous solution under indoor fluorescent light illumination by BiOBr/Bi ₂ S ₃ -60 composite.	148
Figure 6.15	Effect of various scavengers on photocatalytic efficiency (a) kinetic curves (b) of BiOBr/Bi ₂ S ₃ -60 composite towards CIP degradation under indoor fluorescent light illumination.....	149
Figure 6.16	Effect of inorganic salts on the degradation of CIP in the presence of BiOBr/Bi ₂ S ₃ -60 composite.....	151
Figure 6.17	TOC removal in the presence of BiOBr/Bi ₂ S ₃ -60 composite.....	152

Figure 6.18	Proposed mechanism for the photocatalytic degradation of CIP over BiOBr/Bi ₂ S ₃ -60 composite under indoor fluorescent light illumination.	153
Figure 6.19	(a) Recovery test exhibited by BiOBr/Bi ₂ S ₃ -60, and (b) kinetic curves.....	155
Figure 6.20	Recycling performance of photocatalytic degradation of CIP over BiOBr/Bi ₂ S ₃ -60 composite under indoor fluorescent light illumination.	157
Figure 6.21	FTIR spectra of BiOBr/Bi ₂ S ₃ -60 before and after photocatalytic degradation of CIP (reuse five times).....	157
Figure 7.1	Photographs of pristine CA and BCA composite films loaded with different weight percent's of BiOBr.	159
Figure 7.2	XRD patterns of as-synthesized (a) pristine and BCA composite films, (b) enlarged view of diffraction region between 30° - 40°.	160
Figure 7.3	FESEM images of (a) pristine BiOBr, (b, c) pristine CA film, (d) BCA-10, (e) BCA-20, (f) BCA-30 and (g) BCA-40 composite films.	162
Figure 7.4	ATR-FTIR spectra of pristine BiOBr, pristine CA film and BCA composite films	167
Figure 7.5	UV-vis diffuse reflectance spectra of pristine BiOBr, pristine CA film and BCA composite film.....	168
Figure 7.6	TG curves of pristine BiOBr, pristine CA film and BCA composite films	170
Figure 7.7	Effect of BiOBr catalyst loading on the photocatalytic degradation of CIP (20 mg/L, pH 7.1 ± 0.05) using BCA composite films (3 × 3 cm) under indoor fluorescent light illumination.....	171
Figure 7.8	(a) Pseudo-first order kinetic and (b) pseudo-second order kinetic plot for the degradation of CIP using BCA composite films under indoor fluorescent light illumination.....	172
Figure 7.9	(a) Effect of BCA-30 composite film size and (b) their pseudo first order kinetic plot for the photocatalytic degradation of CIP under indoor fluorescent light illumination.....	175

Figure 7.10	(a) Effect of pH on the photocatalytic degradation of CIP using BCA-30 composite film under indoor fluorescent light illumination and (b) their pseudo-first order kinetic plot.....	177
Figure 7.11	(a) Effect of scavengers on the photocatalytic degradation of CIP using of BCA-30 composite film under indoor fluorescent light illumination and (b) their pseudo-first order kinetic plot.....	180
Figure 7.12	TOC removal in the presence of BCA-30 composite film.	181
Figure 7.13	Proposed mechanism for the photocatalytic degradation of CIP over BCA-30 composite film under indoor fluorescent light illumination.	183
Figure 7.14	Recyclability test of the BCA-30 composite film in the photocatalytic degradation of CIP.	184
Figure 7.15	ATR-FTIR spectra of BCA-30 composite film before, during and after photocatalytic reactions.	186

LIST OF ABBREVIATIONS

A	Absorbance
AA	Ascorbic Acid
AB1	Acid Black 1
ATR	Attenuated Total Reflection
BET	Brunauer – Emmet – Teller
BiOBr	Bismuth Oxybromide
BJH	Barret – Joyner – Halenda
BZF	Bezafibrate
CA	Cellulose Acetate
CB	Conduction Band
CR	Congo Red
CQDs	Carbon Quantum Dots
Hg	Mercury
CIP	Ciprofloxacin
DRS	Diffuse Reflectance Spectroscopy
E%	Percent Efficiency
EDS	Energy Dispersive X-ray Spectroscopy
eV	Photon Energy
e^-	Negatively Charged Electron
FESEM	Field Emission Scanning Electron Microscopy

FTIR	Fourier Transform Infra-Red
h^+	Positively Charged Hole
IUPAC	International Union of Pure and Applied Chemistry
ILs	Ionic Liquids
IPA	Isopropyl Alcohol
JCPDS	Joint Committee on Powder Diffraction Standards
K _{sp}	Solubility Product Constant
k_1	Pseudo-First Order Rate Constant
k_2	Pseudo-Second Order Rate Constant
Min	Minutes
mL	Milliliter
MO	Methyl Orange
MG	Malachite Green
MB	Methylene Blue
N ₂	Nitrogen
NAA	Nitrogen Adsorption Analysis
NOR	Norfloxacin
$O_2^{\bullet-}$	Superoxide Radical
OH^{\bullet}	Hydroxyl Radical
pH _{pzc}	pH of Point of Zero Charge
PZC	Point of Zero Charge
PL	Photoluminescence

PMMA	Poly(methyl methacrylate)
PEG 400	Polyethylene Glycol 400
PPM	Parts Per Million
RhB	Rhodamine B
R ²	Correlation Coefficient
SPR	Surface Plasmon Resonance
TCP	Trichlorophenol
TAA	Thioacetamide
TGA	Thermogravimetric Analysis
TOC	Total Organic Carbon
UV	Ultraviolet
UV-Vis	Ultraviolet and Visible
VB	Valence Band
W	Watt
WWTPs	Wastewater Treatment Plants
wt%	Weight Percent
XRD	X-ray Diffraction
XPS	X-ray Photoelectron Spectroscopy

**SINTESIS FOTOMANGKIN BERASASKAN BISMUT OKSIBROMIDA
PADA SUHU BILIK UNTUK PENYINGKIRAN CIPROFLOKSACIN
DARIPADA LARUTAN AKUEUS DI BAWAH CAHAYA NAMPAK**

ABSTRAK

Fotopemangkinan semikonduktor menggunakan fotopemangkin cahaya nampak semakin menarik perhatian kerana penggunaannya yang meluas dalam pertukaran tenaga dan pemulihan alam sekitar. Baru-baru ini, suatu semikonduktor ternari V-VI-VII, bismut oksibromida (BiOBr) telah mendapat perhatian meluas dalam bidang fotopemangkinan kerana kosnya yang rendah, tiada ketoksikan, dan ciri-ciri unik yang lain. Namun, BiOBr mempamerkan kecekapan fotodegradasi yang rendah, kerana penyerapan cahaya nampak yang rendah dan penggabungan semula pembawa cas fotogenerasi. Tambahan lagi, untuk aplikasi praktikal dan berskala besar, pengasingan serbuk BiOBr adalah sukar. Matlamat utama kajian ini adalah untuk mensintesis fotopemangkin berasaskan BiOBr pada suhu bilik, menggunakan cara yang mudah, murah dan mesra alam, untuk meningkatkan aktiviti fotodegradasi BiOBr dan juga untuk memudahkan proses pemisahan fotopemangkin BiOBr dari larutan akueus. Bagi mencapai matlamat ini, dua strategi telah digunakan. Pertama, BiOBr tulen telah digunakan sebagai bahan perumah untuk menghasilkan komposit fotopemangkin. Melalui kedah ini, tiga komposit fotopemangkin berasaskan BiOBr iaitu Bi/BiOBr, BiOBr/Bi₂O₃ dan BiOBr/Bi₂S₃ telah dihasilkan. Kedua, BiOBr tulen telah dipegunkan ke atas selulos asetat (CA), membentuk lapisan komposit BiOBr/selulos asetat (BCA). Struktur dan sifat fizikokimia kedua-dua serbuk dan BiOBr komposit terpegun telah dicirikan menggunakan pelbagai teknik. Setelah itu,

aktiviti fotopemangkin kedua-dua komposit BiOBr terampai dan terpegun telah dikaji menggunakan larutan antibiotik ciprofloksasin (CIP) 20 mg/L, di bawah keadaan makmal yang normal, iaitu pada suhu bilik, pH natural dan, menggunakan lampu pendarfluor padat sebagai sumber cahaya nampak. Dalam kes komposit berasaskan BiOBr serbuk, prestasi optimum dicapai menggunakan komposit Bi/BiOBr-20, BiOBr/Bi₂O₃-60 dan BiOBr/Bi₂S₃-60 dengan kadar degradasi bagi BiOBr/Bi₂S₃-60 > Bi/BiOBr-20 > BiOBr/Bi₂O₃-60. Tambahan lagi, faktor peningkatan bagi Bi/BiOBr-20, BiOBr/Bi₂O₃-60 dan BiOBr/Bi₂S₃-60 berbanding BiOBr tulen masing-masing adalah 4.75, 4.14 dan 5.9. Kesan tersebut dikaitkan terutamanya kepada pemisahan pembawa cas fotogenerasi yang lebih baik dan peningkatan penyerapan cahaya nampak. Untuk lapisan komposit BCA, walaupun kadar tindak balas didapati lebih rendah berbanding sistem berasaskan BiOBr terampai, kadar tindak balas didapati meningkat dengan peningkatan saiz lapisan. Oleh itu, selain daripada aplikasi dan pemisahan lapisan komposit yang mudah, penyerakan cahaya yang mengurangkan aktiviti fotopemangkinan pada muatan tinggi dapat minimumkan. Secara umumnya, kinetik degradasi fotopemangkin bagi semua komposit berasaskan BiOBr mematuhi model pseudo tertib pertama dan lubang (h^+) serta radikal anion superoksida ($\bullet O_2^-$) dikenalpasti sebagai spesies degradasi utama. Seterusnya mekanisme bagi degradasi CIP menggunakan fotopemangkin komposit berasaskan BiOBr serbuk dan lapisan BCA telah dicadangkan. Semua komposit kekal stabil iaitu sehingga 5 kitaran bagi komposit berasaskan BiOBr terampai dan sehingga 10 kitaran bagi sistem dengan lapisan BCA. Akhir sekali, dipercayai bahawa kajian ini menawarkan suatu kaedah yang efisien dan mudah untuk mensintesis bahan berasaskan bismut oksihalida untuk aplikasi tenaga dan juga alam sekitar.

**ROOM-TEMPERATURE SYNTHESIS OF BISMUTH OXYBROMIDE-
BASED PHOTOCATALYSTS FOR THE REMOVAL OF CIPROFLOXACIN
FROM AQUEOUS SOLUTION UNDER VISIBLE LIGHT**

ABSTRACT

Semiconductor photocatalysis using visible-light-driven photocatalysts is gaining more attention, due to its wide applications in energy conversion and environmental remediation. Recently, a ternary V-VI-VII semiconductor, bismuth oxybromide (BiOBr) has received extensive attention in photocatalysis due to its low cost, non-toxicity, and other unique properties. However, BiOBr alone exhibits low photodegradation efficiency, due to low visible light absorption and recombination of photogenerated charge carriers. Furthermore, for practical and large-scale application, the separation of powdered BiOBr is inconvenient. The primary aims of this work are to synthesize BiOBr-based photocatalysts at room-temperature, using facile, low cost and environmentally friendly methods, to enhance the photodegradation activity of BiOBr, as well as to ease the separation of the photocatalyst from the aqueous system. To achieve these goals, two strategies were employed. First, the pristine BiOBr was used as a host material to produce photocatalyst composites. Using this method, three BiOBr-based composites namely Bi/BiOBr, BiOBr/Bi₂O₃ and BiOBr/Bi₂S₃ were prepared. Second, the pristine BiOBr was immobilized onto cellulose acetate (CA), forming BiOBr/cellulose acetate (BCA) composite films. The structural and physicochemical properties of both powdered and immobilized BiOBr-composites were characterized using various techniques. Thereafter, the photocatalytic activities of both suspended and immobilized BiOBr-composites were evaluated by using a

solution of 20 mg/L ciprofloxacin (CIP) antibiotic, under normal laboratory conditions, which is at room-temperature, natural pH and, using compact fluorescent light as the visible – light source. In the case of powdered BiOBr-based composite photocatalysts, optimum performance was achieved using Bi/BiOBr-20, BiOBr/Bi₂O₃-60 and BiOBr/Bi₂S₃-60 composites, with the degradation rate of BiOBr/Bi₂S₃-60 > Bi/BiOBr-20 > BiOBr/Bi₂O₃-60. Moreover, the enhancement factors for Bi/BiOBr-20, BiOBr/Bi₂O₃-60 and BiOBr/Bi₂S₃-60 composites over pristine BiOBr are 4.75, 4.14 and 5.9, respectively. Such effect is attributed mainly to the better separation of photogenerated charge carriers and improved visible light absorption. As for the BCA composite films, although the reaction rate was much slower compared to the suspended BiOBr-based systems, the reaction rate was found to improve with the increase in film size. Therefore, apart from the convenient application and separation of the composite films, light scattering which reduces the photocatalytic activity at higher loading has been reduced. In general, the kinetics of photocatalytic CIP degradation using all the BiOBr-based composites fit the pseudo-first-order kinetic model while, holes (h^+) and superoxide radical anions ($\bullet\text{O}_2^-$) were found to be the dominant degrading species. Thus, the mechanism for the degradation of CIP using the BiOBr-based composite and the BCA film was proposed. Furthermore, all the composite systems remained stable over the cycles investigated, which was five cycles for the suspended BiOBr-based composites and ten cycles for the BCA films system. Finally, it is believed that this work provides an efficient avenue for the facile synthesis of other bismuth-based materials for energy and environmental applications.

CHAPTER 1

INTRODUCTION

1.1 Background

Water is a very vital resource upon which all life on the planet depends on for sustenance. Currently, due to industrialization and increase in human population, the need for this resource continues to increase. Unfortunately, activities related to industrial, clinical, agricultural, domestic and others have paved way for water pollution, thereby making the supply of clean water difficult. A recent projection by United Nations reveals that, between 1/2 and 2/3 of the world's population would experience scarcity of fresh water in 2025 (Barlow and Clarke, 2017).

Nowadays, the detection of pharmaceuticals as pollutants in water bodies is a global phenomenon. Among the pharmaceuticals, antibiotics are highly prescribed medications worldwide, with consumption of around 200,000 tons annually (Sun *et al.*, 2012). Such large-scale use of antibiotics is a threat to both human health and ecosystem, because of their partial metabolism after consumption, which leads to their recurrent detection in hospital waste or excreta (Yang *et al.*, 2016). The presence of antibiotics in water bodies attracts some negative consequences including short and long-term toxicity, endocrine disrupting effects and resistance of antibiotics by microorganisms. Unfortunately, as reported by the United State Environmental Protection Agency (USEPA), the conventional treatment techniques employed by most wastewater treatment plants (WWTPs) are not efficient for the treatment of wastewater contaminated by pharmaceuticals (Tay and Madehi, 2015). This makes the search for efficient water treatment technologies, an issue of urgent importance.

Among many potential solutions to this problem, photocatalytic based treatment, using semiconductor turns out to be a fascinating technique, because it is economical, safe, nontoxic and renewable. While TiO_2 is widely known and used, bismuth oxybromide (BiOBr) is now receiving attention from various researchers. And, unlike TiO_2 which is inactive under visible light, BiOBr absorbs a fraction of visible light, which makes it a more promising photocatalyst. However, it is expected that, the use of BiOBr could be elevated by enhancing its visible light response, inhibiting its electron-hole recombination or making its application convenient.

Previous studies have reported that, methods such as doping of transition metals including iron (Yuan *et al.*, 2017) and zinc (Guo *et al.*, 2019a), or rare earth metals such as lanthanum (Yin *et al.*, 2017), cerium (Hu *et al.*, 2019) and erbium (Liu *et al.*, 2017a), or formation of heterojunction between BiOBr and other semiconductors such as $\text{Bi}_2\text{O}_2\text{CO}_3$ (Qiu *et al.*, 2017), BiPO_4 (Zou *et al.*, 2017) or FeWO_4 (Gao *et al.*, 2018) are effective towards improving the performance of BiOBr. These strategies enhance the photocatalytic performance of BiOBr by improving its optical absorption or inhibiting the recombination of charge carriers or both. Similarly, the polymer-supported photocatalyst system has remained one of the best approaches that is been employed to rectify the problems encountered during application and recovery of photocatalysts. For this purpose, polymers matrices such as polyethersulfone (PES) (Hir *et al.*, 2017) and cellulose acetate (CA) (Jin *et al.*, 2014) have been used in the preparation of composite films with better flexibility and recyclability.

1.2 Problem Statements

The presence of antibiotics such as ciprofloxacin (CIP) in water bodies is a clear threat. This is because, in addition to water pollution and their slower rate of photolytic decay, long term presence of antibiotics in water bodies leads to the development of antibiotic-resistant bacterial strains (Kumar *et al.*, 2019). Also, unlike dyes which act as photosensitizers by facilitating their degradation process under visible light, antibiotics have absorbance in the UV region, and therefore could not act as photosensitizers under visible light, thus making their degradation process purely photocatalytic under visible light.

Photocatalytic degradation under solar irradiation has been widely explored. However, challenges during bad weather made it necessary to search for a suitable and promising alternative. In view of that, the prolonged lifetime, convenience and safety of indoor fluorescent light, makes it a paramount option.

Besides TiO_2 , recently discovered photocatalysts such as BiOBr could also be considered for the removal of antibiotics, such as CIP from aqueous solution under indoor light irradiation. However, prior to that, challenges of BiOBr such as low visible light absorption and recombination of charge carriers' needs to be addressed.

Finally, the application of photocatalysts in powdered form for large-scale water remediation is often discouraged by the post-reaction separation process, having combine challenge of energy and time consumption. Moreover, suspension of photocatalysts could result in light scattering leading to reduced photodegradation efficiency. Immobilizing BiOBr onto a substrate is one of the alternatives to overcome these problems.

1.3 Objectives of the Proposed Study

1. To synthesize various BiOBr-based photocatalysts at room-temperature using solid-state synthesis and in-situ modification/immobilization and characterize their structural and physicochemical properties using various methods.
2. To determine the efficiency of BiOBr-based photocatalysts towards removal of ciprofloxacin (CIP), an antibiotic, from aqueous solution.
3. To establish the kinetics and mechanism of the removal of CIP from aqueous solution using BiOBr-based photocatalysts.
4. To correlate the catalytic activity of BiOBr-based photocatalysts with their physicochemical properties.

1.4 Scope and Limitations of the Study

The present study covers the development of BiOBr-based photocatalysts, their characterization and application for the photocatalytic removal of ciprofloxacin from aqueous system, under visible light. The development of BiOBr includes doping with a non-noble metal (bismuth), formation of heterojunction with bismuth oxide (Bi_2O_3), formation of heterojunction with bismuth sulphide (Bi_2S_3) and immobilization via formation of a composite film using cellulose acetate (CA). The formed BiOBr-based composite photocatalysts were then characterized using various methods. However, their photocatalytic activity was only assessed via degradation of CIP and under compact fluorescent light as the only visible light source. A schematic framework of the work conducted in this thesis is shown in Figure 1.1.

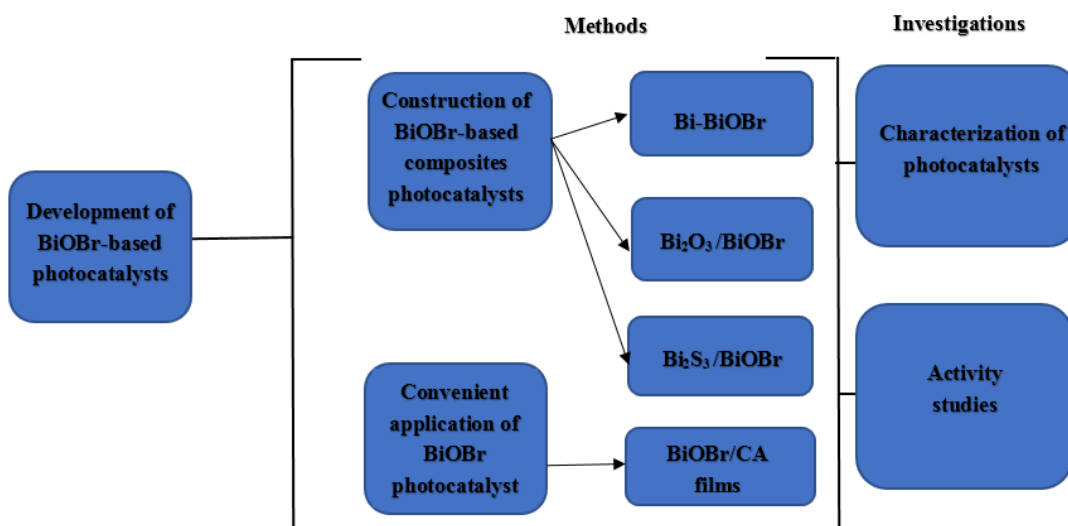


Figure 1.1: Framework of the thesis

1.5 Outline of the Thesis

This thesis has been structured into 8 chapters. The first chapter presents an overview of the work, including the problem statements, research objectives and scope of the study. The second chapter provides a literature review of the topic. The methodology of the work was elaborated in the third chapter, including chemicals used during synthesis and activity studies, together with the instruments employed for the characterizations. In chapters four, five and six, the characterization of structural, morphological, functional groups, textural, optical, as well as the findings on the application Bi/BiOBr, Bi₂O₃/BiOBr and Bi₂S₃/BiOBr composites on the removal of CIP from aqueous solution are discussed and compared, respectively. In the seventh chapter, the characterization of structural, morphological, functional groups, thermal, optical, as well as the findings on the application of BiOBr/CA composite films on the removal of CIP from aqueous solution are discussed and compared. Finally, chapter eight concludes the major findings during the course of this research and presents some recommendations for future work in this field.

CHAPTER 2

LITERATURE REVIEW

2.1 Background

Pharmaceuticals and personal care products (PPCPs) are extensively used in people's daily life and other fields for various purposes including medical, industrial, aquaculture, livestock industry etc. The consumption volume of PPCPs is very high that, even their estimated annual production falls above 2×10^7 tons (Wang and Wang, 2016). Such extensive use explains their presence in ground water, surface water, industrial and municipal effluents. The first reported case for the detection of PPCPs in surface water in Europe and United States was in the 1960s (Stumm-Zollinger and Fair, 1965). Since then, several literatures have reported the detection of PPCPs with concentration ranging from ng/L to several $\mu\text{g/L}$ in surface, ground and drinking water worldwide (Hao *et al.*, 2019; Wang and Chu, 2016; Yang *et al.*, 2017c). Their source have mainly been traced to come from domestic wastewater, livestock excretion, hospital wastewater, wastewater from pharmaceutical industries or from expired PPCPs being discharged into the environment (Elmolla and Chaudhuri, 2011; Martinez Gomez *et al.*, 2015). The presence of PPCPs in drinking water demonstrate the incapability of the techniques employed by most wastewater treatment plants (WWTPs) in treating wastewater contaminated by PPCPs. For instance, studies by Kosma *et al.* (2014) have reported the presence of PPCPs in the influents and effluents of WWTPs in Greece at concentration levels ranging from 9.3 to 96648.3 ng/L and 6.6 to 1076 ng/L, respectively. In view of the potential threats of such polluted waters to both human health and the environment, more effective wastewater remediation techniques are urgently needed.

2.2 Advanced Oxidation Processes (AOPs) for Wastewater Treatment

The use of advanced oxidation processes (AOPs) including Fenton process, ultraviolet/hydrogen peroxide process (UV/H₂O₂), ozonation, electrochemical oxidation, photo-Fenton process and semiconductor photocatalysis in the purification of portable water began in the 1980's (Deng and Zhao, 2015). Since then, the processes have been regarded as the ultimate, due to their unique ability of destructing organic contaminants in wastewater into harmless end-products. Although, the AOPs varies in their reacting systems, their common feature involves the use of oxidizing species like hydroxyl radicals ($\bullet OH$) in degrading targeted compounds through either homogeneous or heterogeneous process. However, the difficulty in separating the catalyst from the reaction system in homogeneous process, makes heterogeneous process more convenient. In view of its advantages, heterogeneous photocatalysis, or in other words referred to as semiconductor photocatalysis, is now widely investigated for use in wastewater remediation.

2.3 Semiconductor Photocatalysis

A semiconductor is a material having electrical conductivity greater than that of an insulator (e.g. wood), but below that of a conductor (e.g. metals). The material could initiate a photocatalytic reaction, after being irradiated with light of sufficient energy. Semiconductor photocatalysis is a reaction whereby a semiconductor under ultraviolet, visible or infrared radiation absorbs a quanta of light to produce species which alters or initiates a chemical reaction, and is involved in the chemical transformation of the reaction partner (Braslavsky, 2007). The essential elements of a photocatalytic reaction are: (i) a light source, (ii) a photocatalyst, and (iii) the chemical transformation of the reaction partners. It should be noted that, a semiconductor photocatalyst needs to be chemically and biologically inert, photoactive and photo-

stable, inexpensive and ecologically friendly, in order to promote its practical application (Choi, 2016).

In the 1970s, water splitting reaction using TiO_2 electrodes by Fujishima and Honda (1972), initiated a new era for semiconductor photocatalysis. Such milestone-like discovery paved way for the diverse application of semiconductor photocatalysis in the area of energy and environment. Although, different semiconductors have different light or energy requirements, the common requirement of semiconductors in a photocatalytic reaction is that, the energy ($h\nu$) of the photons should be sufficient and enough to excite electrons from valence band (VB) to the conduction band (CB) of the particular semiconductor. Bandgap (E_g) is the name given to the empty energy region between the valence and conduction band of a semiconductor (Nyankson *et al.*, 2013). In addition to the E_g , the position of the VB and the position of the CB are important features that determine the photocatalytic ability of a semiconductor (Yang *et al.*, 2008).

Metal oxides including the renowned TiO_2 are the most widely used semiconductor photocatalysts. However, due to its wide bandgap (3.2 eV), TiO_2 is only active under ultraviolet light, which constitutes about 3 – 5% of the total energy from the sunlight. The high percentage of visible light energy from the sun now encourages the search for more visible-light-active photocatalysts (Xu *et al.*, 2015).

A schematic illustration of a typical photocatalytic process is shown in Figure 2.1. Generally, a photocatalytic reaction gets initiated upon illumination of a semiconductor photocatalyst with $h\nu$ greater than its E_g , leading to the generation of highly reactive electron (e^-) – hole (h^+) pairs. The photogenerated charge carriers subsequently undergoes one of the three possible processes; (1) instantly recombine

by dissipating energy in the form of heat or light, (2) get trapped at defect sites or (3) move to the surface of the semiconductor in order to initiate redox reaction with adsorbates (Xu *et al.*, 2015). Unfortunately, the first two processes reduce the availability of photogenerated charge carriers, thereby inhibiting the photocatalytic activity. The third process is the main pathway to photocatalytic activity. It is important to point out that, the concentration of charge carriers on the surface of the semiconductor photocatalyst highly depends on the intensity of incident light and the efficient separation of photogenerated charge carriers by preventing their recombination. Such factors are paramount towards achieving better performance during photocatalytic activity.

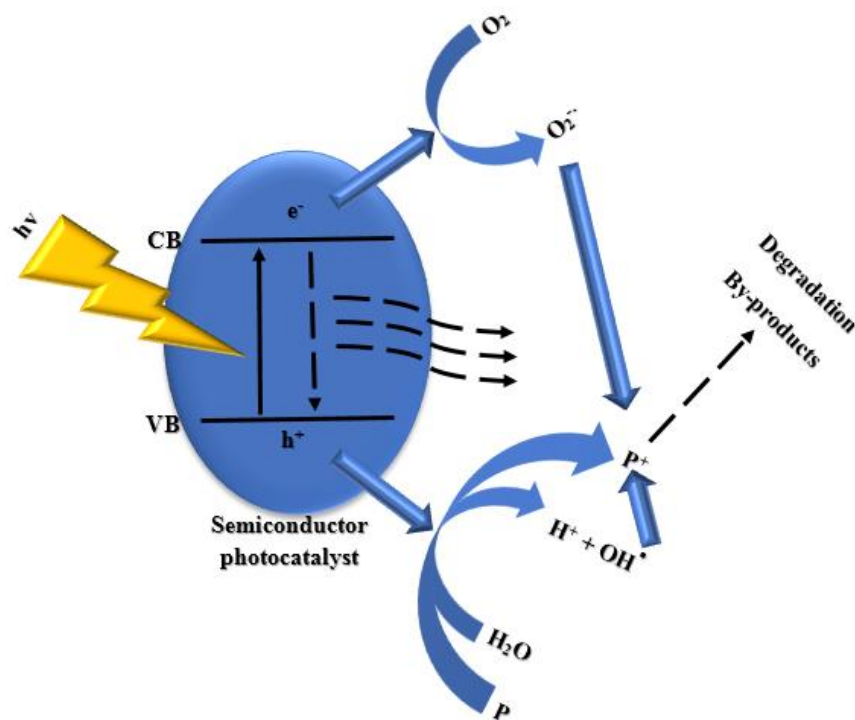
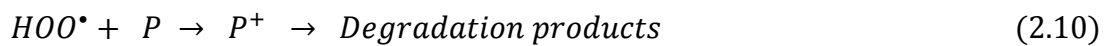
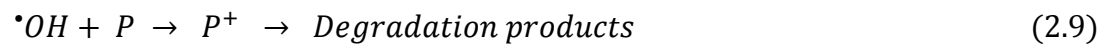
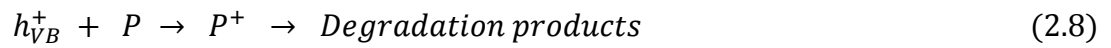
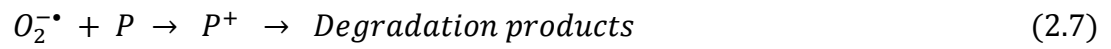
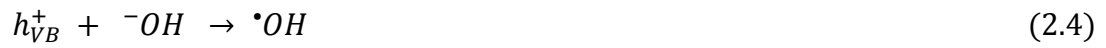
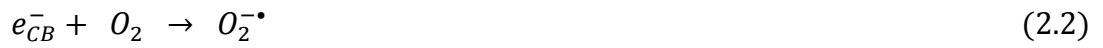
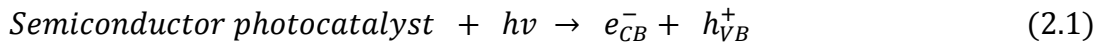


Figure 2.1: Schematic illustration for the generation of oxidative species in a photocatalytic reaction (Chong *et al.*, 2010).

After the successful transfer of photogenerated charge carriers to the surface of the semiconductor, the electrons (e_{CB}^-) are scavenged by oxygen (O_2), producing superoxide radical anion ($O_2^{\bullet-}$). Protonation of $O_2^{\bullet-}$ subsequently leads to the formation of hydroperoxyl radicals ($\bullet OOH$) and then hydrogen peroxide (H_2O_2) (Pelaez *et al.*, 2012). Such generated superoxide radical anions and hydroxyl radicals participate directly in the degradation of organic pollutants (P). The holes (h_{VB}^+) on the other hand are capable of either directly oxidizing P to produce degraded products (P^+), or H_2O to produce hydroxyl radicals ($\bullet OH$). Equations 2.1 to 2.10 below explains the proposed mechanism of a typical photocatalytic reaction (Chong *et al.*, 2010).



2.4 Reaction Kinetics

The Langmuir-Hinshelwood model (LHM) is the commonly used model in explaining the kinetics for the heterogeneous photocatalytic degradation of organic matter. The main assumption of LHM is that reactants are adsorbed on the active sites of the catalyst surface before commencement of the reaction (Loghambal *et al.*, 2018).

The LHM equation is given below:

$$r = - \frac{dC}{dt} = \frac{k_r KC}{1 + KC} \quad (2.11)$$

where r is the degradation rate (dC/dt), k_r is the reaction rate constant, K is the adsorption coefficient of the organic pollutant and C is the reactant concentration.

when the concentration of the substances exceeds the saturation coverage of the catalyst surface (i.e. $KC \gg \gg 1$), equation 2.11 becomes a zero-order expression (equation 2.12).

$$r = - \frac{dC}{dt} = k \quad (2.12)$$

when the concentration of the substrate is very low (i.e. $KC \ll \ll 1$), equation 2.11 becomes:

$$r = - \frac{dC}{dt} = k_r KC \quad (2.13)$$

Integrating equation 2.13 with respect to the limits $C = C_o$ at $t = 0$ and $C = C_t$ at $t = t$, reduces the equation to the pseudo-first order kinetic as given by equation 2.14:

$$\ln \left(\frac{C_o}{C_t} \right) = k_r K t = k t \quad (2.14)$$

where k is the pseudo-first order rate constant.

2.5 Bismuth-Based Compounds

Bismuth (Bi) is a white substance discovered in the 1660s, and is the 64th most abundant element on the earth's crust (Salimi *et al.*, 2018). It belongs to the category of heavy metals and has an atomic mass of 208.980. Although, Bi mostly occurs in its native state, however, other important ores of Bi are bismite (bismuth oxide, Bi₂O₃) and bismuthinite (bismuth sulfide, Bi₂S₃), or even as byproduct in lead, tin and copper mining (Bothwell *et al.*, 2011). Fortunately, unlike other heavy metals such as lead and arsenic which are highly toxic, bismuth is non-toxic and non-carcinogenic. According to Suzuki *et al.* (2001), table salt is even more toxic than many of bismuth compounds. For such reason, bismuth is now being regarded as a green element (Hernandez-Delgado *et al.*, 2018; Jovanovski *et al.*, 2017; Liang *et al.*, 2019).

Bismuth-based compounds are inexpensive and have been used for over four centuries, in many applications including cosmetics, medicines and pigments. For instance, bismuth subsalicylate is used as an active ingredient in making antidiarrheal drugs e.g. Peptobismol (Saunders, 2010), bismuth oxychloride is used in cosmetics (Maile *et al.*, 2005), bismuth subnitrate is used during surgeries as an antiseptic (Bothwell *et al.*, 2011), while bismuth vanadate is used as a pigment in paints (Patil *et al.*, 2016). Currently, many researches are ongoing, with the aim of evaluating bismuth as a non-toxic replacement for lead in several applications (Lyu *et al.*, 2017).

Over the last decade, the rising environmental concern has facilitated the tremendous demand for green catalysts. Currently, many researches have focused towards the application of many bismuth-based compounds including BiOBr, Bi₂WO₆, BiOI etc. as catalysts in organic synthesis (Banerjee, 2017), hydrogen production (Lee *et al.*, 2018), wastewater purification (Abazari *et al.*, 2019) and many other applications (Meng and Zhang, 2016).

2.6 Bismuth Oxybromide (BiOBr)

Bismuth oxybromide (BiOBr) is p-type semiconductor having an indirect-transition band gap between 2.64 – 2.91 eV (Li *et al.*, 2015b). It is chemically stable and among the group of V-VI-VII ternary semiconductors. Various shaped BiOBr including nanobelts (Li *et al.*, 2016a), nanoflowers (Guo *et al.*, 2019a), nanospheres (Chen *et al.*, 2017), and nanoflakes (An *et al.*, 2015) have been synthesized using methods such as solvothermal (Li *et al.*, 2016a), ionothermal (Zhang *et al.*, 2012), hydrothermal (Sin *et al.*, 2017) and co-precipitation synthesis (Kong *et al.*, 2012). Currently, BiOBr is been used for various purposes including water splitting (Guo *et al.*, 2019a), indoor-gas purification (Ai *et al.*, 2011), photocatalytic wastewater treatment (Wang *et al.*, 2018c) and selective oxidation of alcohol (Yuan *et al.*, 2017).

BiOBr belongs to a series of BiOX (X = F, Cl, Br, I), which crystallizes in a tetragonal layered structure consisting of $[\text{Bi}_2\text{O}_2]$ slabs doubly interleaved by slabs of $[\text{X}]$ atoms, to form $[\text{Bi}_2\text{O}_2\text{X}_2]$ layers along the c axis (Guo *et al.*, 2016a). The Bi center in each layer (Figure 2.2), is surrounded by four oxygen atoms with strong covalent bonds, and with four halogen atoms having weak interlayered van der Waals interactions. Compared to the bismuth and oxygen atoms that are bonded together through a strong covalent bond, the weak van der Waals interactions of the double halogen slabs, makes the halogen atoms instable and active. Furthermore, due to the strong intralayer and weak interlayer interactions of the $[\text{Bi}_2\text{O}_2]$ slabs and the double $[\text{X}]$ slabs in the layered BiOX structure, charge distribution between $[\text{Bi}_2\text{O}_2]$ and $[\text{X}]$ slabs are non-uniform, as a result of which the related atoms and orbitals could be polarized. Sequel to that, the possibility of an induced internal electric field (IEF) along the perpendicular crystal orientation exists. Such IEF feature could play a vital

role by inhibiting the recombination of photogenerated charge carriers during photocatalysis (Zhao *et al.*, 2016b).

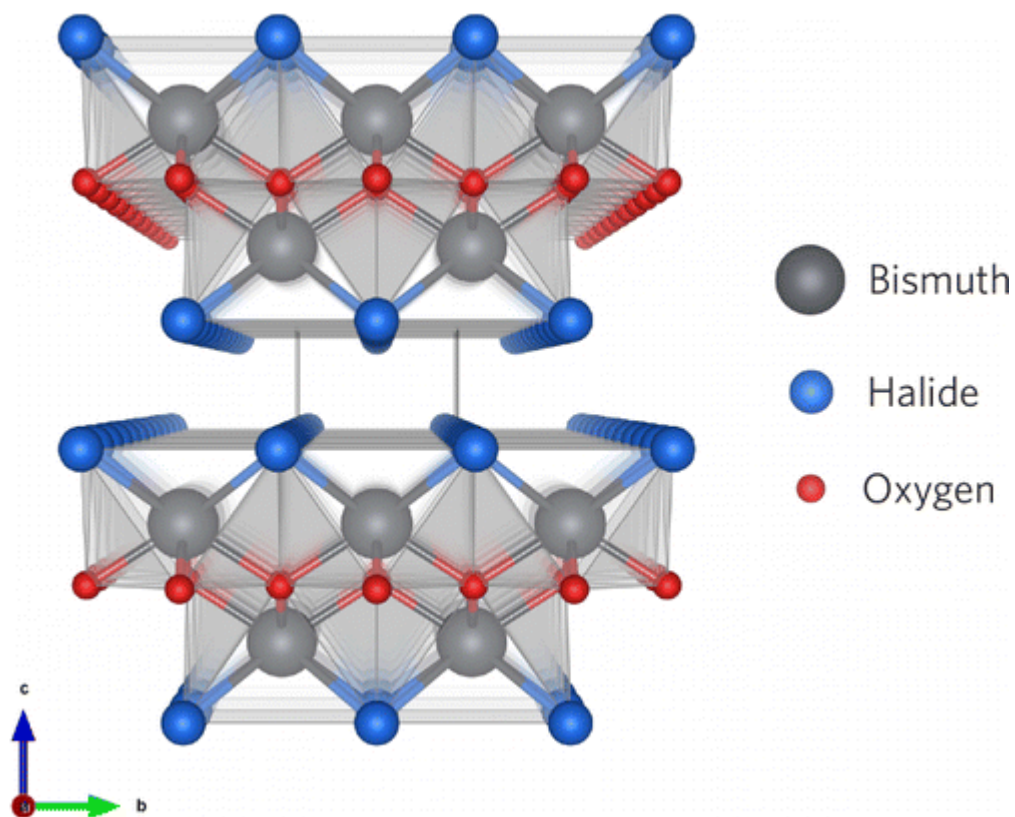


Figure 2.2: Crystal structure of BiOX (X = F, Cl, Br, I) systems (Ganose *et al.*, 2016).

2.7 Synthesis of BiOBr

Despite the possibility for the commercial supply of BiOBr by industries, the choice of some specific target features, including crystallinity, morphology, particles size, surface area etc. have inspired the synthesis of various forms of BiOBr using many laboratory techniques. Over the years, many methods including solvothermal, hydrothermal, ionothermal co-precipitation, microwave-assisted and hydrolysis method have been used to synthesize BiOBr and are discussed in the following sections.

2.7.1 Solvothermal and Hydrothermal Methods

Solvothermal and hydrothermal synthesis involve subjecting a precursor solution inside an autoclave to thermal treatment. As a result of such thermal treatment, an autogenous pressure inside the autoclave initiates a reaction that otherwise could be hard to achieve under ambient conditions. A unique feature of both processes is that, tuning of kinetic and thermodynamic parameters such as temperature and time of reaction, could allow the precise control of crystal phase, morphology and size.

Previously, Huo *et al.* (2012) have reported the synthesis of BiOBr via solvothermal method, while Jiang *et al.* (2010) have reported the synthesis of BiOBr via hydrothermal method. However, unlike the hydrothermal synthesis which involves the use of an aqueous precursor solution, the solvothermal synthesis employs the use of a wide variety of solvents such as methanol (Vadivel *et al.*, 2014), ethylene glycol (Liu *et al.*, 2014b), glycerol (Liu *et al.*, 2012a) etc. in preparing the precursor solution during synthesis. Variation in solvents during solvothermal synthesis affects the growth direction of BiOBr crystals. However, such solvents might allow the elevation of temperature and pressure compared to hydrothermal method (Liu *et al.*, 2012a). In general, product yield of BiOBr synthesized using solvothermal and hydrothermal methods is usually low.

2.7.2 Ionothermal Method

A very recent modification of the solvothermal method, involves the use of ionic liquids (ILs) as additives or solvents in synthesis. They are non-flammable and non-volatile with unique features such as thermal stability, negligible vapor pressure, tunable properties and designable structures. ILs play important role during the synthesis due to their superior capability for solvation and stabilization of metal cations (Ma *et al.*, 2010).

Zhang *et al.* (2012) synthesized BiOBr via the ionothermal method, using 1-butyl-3-methyl-imidazolium-bromide as both the ionic liquid and as the source of bromide. The end-product was observed to have a 3D hierarchical architecture and exhibited excellent performance in removing heavy metals and dyes. However, just like the solvothermal method, the yield of products synthesized using the ionothermal method is usually low.

2.7.3 Microwave-Assisted Method

Unlike the solvothermal, hydrothermal or ionothermal methods which require long duration for the reaction to reach completion stage, the microwave-assisted synthesis could accelerate the rate of chemical reaction by around 1000-fold times or more (Yang *et al.*, 2015), thereby making the process faster.

For instance, Zhang and Yang (2015) synthesized BiOBr via the microwave-assisted synthesis, using a 200 W JK-MCR-205 microwave reactor and then, the normal solvothermal synthesis method. The efficiency of the microwave-assisted synthesis is so pronounced that, a reaction which requires a temperature of 140 °C maintained for 8 h, to reach completion using the conventional solvothermal method, could be completed in just 10 min via the microwave-assisted method.

2.7.4 Hydrolysis Method

Hydrolysis method is an easy, fast and inexpensive synthesis technique. The process involves complete dissolution of Bi_2O_3 , as the bismuth source, in excess amount of concentrated HBr acid, to form an aqueous system of $\text{BiBr}_3\text{-HBr}$. Subsequently, the concurrent addition of hydrolytic agent and adjustment of the pH of the system to a value ~ 10 , mostly using Na_2CO_3 , results in the formation of BiOBr precipitates. These are then filtered, washed and dried (Shi *et al.*, 2011; Wang *et al.*, 2013).

The nature of BiOBr synthesized using the hydrolysis method are mostly homogeneous plate-like nanoparticles, with high purity, as the energy dispersive x-ray spectroscopy (EDS) analytical results usually reflects the nominal mole ratio of Bi, O and Br atoms. However, the BiOBr products obtained using the hydrolytic method are usually poorly crystalline (Wang *et al.*, 2008).

2.7.5 Co-precipitation Method

Co-precipitation method is another facile preparation process that has been employed for the synthesis of BiOBr . The main feature of the process is that, soluble precursors are being precipitated. It usually requires shorter duration, and takes place at low temperature, compared to solvothermal, ionothermal or hydrothermal methods. The common preparation stages of the co-precipitation method are stirring, aging, filtering/centrifuging, washing and drying. The synthesis of BiOBr using the co-precipitation method has been reported by Lu *et al.* (2012), and the product obtained has a flake-like morphology, with thickness of about 40 nm, and an average diameter of about 300 nm.

2.8 Photocatalytic Enhancement of BiOBr

Despite the unique features of BiOBr, many efforts are still being made to promote its efficiency. Such efforts usually target the enhanced absorption of visible light, or inhibition of photogenerated charge carrier's recombination, or both. Currently, the widely used methods for these purposes include elemental doping and formation of heterojunction with other semiconductors and are discussed in the following section.

2.8.1 Elemental Doping

Incorporation of dopants such as transition metals, rare-earth metals and noble metals into BiOBr have been widely reported in literatures. As tabulated in Table 2.1, different forms of dopants have been used for the enhancement of the photocatalytic efficiency of BiOBr. One of the key observations is that, doping appropriate amount of cations successfully inhibits electron-hole recombination (Liu *et al.*, 2012b). Furthermore, some of the introduced cations also improve other properties, such as the visible light harvesting ability of BiOBr and redox potential of the photogenerated radicals (Tu *et al.*, 2015). However, it is important to note that excess cationic dopants could serve as recombination centers, causing a decrease in photocatalytic activity (Song *et al.*, 2016).

The photocatalytic activity of BiOBr loaded with noble metals have been studied by different researchers. For instance, Meng *et al.* (2018a) studied the photocatalytic activity of Pd-doped BiOBr by dispersing palladium nanoparticles onto the surface of BiOBr, using photodeposition method. Although, the loaded palladium nanoparticles only rested on the surface of BiOBr instead of covalently anchoring to the lattice, the recombination of photogenerated charge carriers was greatly inhibited. Also, absorbance intensity of Pd-doped BiOBr in the visible region was significantly

improved with further loading of palladium nanoparticles, which was attributed to their surface plasmon resonance (SPR) effect. However, despite the slight decrease in surface area from 3.3 m²/g in pristine BiOBr to 2.4 m²/g in 0.5 Pd-BiOBr, the 0.5 Pd-BiOBr catalyst successfully degraded 100% of phenol [10 mg/L] within 300 min, while pristine BiOBr degraded only 67%. Furthermore, silver nanoparticles have also been loaded onto the surface of BiOBr by Li *et al.* (2015a), using the photoreduction process. The Ag/BiOBr composite was able to degrade 98.6% of methyl orange (MO) within 2 h, while pristine BiOBr degraded only 58.5%. The superior photocatalytic performance of Ag/BiOBr was due to the strengthened incident light usage and improved electron-hole separation efficiency.

Besides the noble metals, literatures have also reported the introduction of rare earth metals including La and Er as dopants into BiOBr. For example, the photocatalytic activity of La-doped BiOBr have been studied by Yin *et al.* (2017). Although, the performance of BiOBr was enhanced by doping appropriate amount of La³⁺ ions, higher dosage leads to the formation of recombination center which reduced photocatalytic activity. Similar results were reported when Xia *et al.* (2016b) synthesized a series of 1, 3, 5 and 8 wt% Er-doped BiOBr samples for photocatalytic degradation of ciprofloxacin. The Er-doped BiOBr samples exhibited apparent red shift compared to pristine BiOBr. During application, the photocatalytic efficiency increased from 1 – 3 wt% Er-BiOBr, and then decreased. Such results have clearly showed that, only appropriate doping amount improves photocatalytic performance.

Other form of cationic dopants that were reportedly introduced into BiOBr are the transition metals. The doping of transition metals was also found to improve photoabsorption in the visible region and inhibit electron-hole recombination. For example, Liu *et al.* (2012b) synthesized a series of Fe-doped BiOBr and were applied

for the photocatalytic degradation of methyl orange using 150 W tungsten-halogen lamp as the light source. The photocatalytic efficiency of Fe-doped BiOBr samples was found to be higher than that of pristine BiOBr. This was attributed to the systematic red shift in visible light absorption of the Fe-doped BiOBr composites, and the formation of Fe^{2+} ions and Fe^{4+} ions through the trapping photoinduced electrons and holes by Fe^{3+} ions, a process that inhibits their recombination. Also, Song *et al.* (2016) synthesized a series of Zn-doped BiOBr samples for use as photocatalysts to degrade rhodamine B dye, under 300 W Xe lamp. Although, the absorption edge of the Zn-doped BiOBr samples was shifted slightly to higher wavelengths with the increase in zinc contents, only appropriate amount of zinc doped into BiOBr results in enhanced photodegradation efficiency.

Apart from cationic dopants, literatures have also reported the introduction of anionic dopants into BiOBr. For instance, the photocatalytic activity of B-doped BiOBr samples have been reported by Liu *et al.* (2016b). Both pristine and a series of 0.02, 0.05, 0.07 and 0.1 (values represent molar ratio of B to Bi) B-doped BiOBr samples were reported to have the same absorption curves with an absorption edge of ~ 440 nm, an indication that B dopant has little effect on the visible-light response. However, on application, the 0.07 B-doped BiOBr displayed the highest efficiency for the photocatalytic degradation of RhB, while a decrease in efficiency was observed by 0.1 B-doped BiOBr sample, an effect attributed to recombination of photogenerated carriers.

Table 2.1: Comparative degradation efficiencies of various pristine and doped BiOBr photocatalysts

Dopant	Light source/pollutant	Experimental conditions Dosage; [pollutant]; irradiation time	Photodegradation efficiency (%)		References
			BiOBr	Doped BiOBr	
Pd	300 W halogen tungsten projector lamp / Phenol	1 g/L; [Phenol] = 10 mg/L; 300 min	67	100	Meng <i>et al.</i> (2018a)
La	300 W Xenon lamp / CIP	0.1 g/L; [CIP] = 10 mg/L; 180 min	28	48	Yin <i>et al.</i> (2017)
Er	300 W Xenon lamp / CIP	0.1 g/L; [CIP] = 10 mg/L; 360 min	50	61	Xia <i>et al.</i> (2016b)
Zn	300 W Xenon lamp / RhB	0.5 g/L; [RhB] = 2×10^{-5} mol/L; 15 min	57	100	Song <i>et al.</i> (2016)
Sn	500 W Xenon lamp / RhB	0.2 g/L; [RhB] = 10 mg/L; 120 min	~ 40	~ 70	Tu <i>et al.</i> (2015)
Ag	500 W Xenon lamp / MO	0.2 g/L; [MO] = 10 mg/L; 120 min	58.5	98.6	Li <i>et al.</i> (2015a)
Fe	150 W tungsten-halogen lamp / MO	1 g/L; [MO] = 10 mg/L; 120 min	75	100	Liu <i>et al.</i> (2012b)
Sn	300 W Xenon lamp / CIP	0.4 g/L; [CIP] = 20 mg/L; 40 min	~80	~97	Xu <i>et al.</i> (2019b)
B	150 W tungsten-halogen lamp / RhB	1 g/L; [RhB] = 15 mg/L; 30 min	71.1	99.3	Liu <i>et al.</i> (2016b)

* CIP = Ciprofloxacin; RhB = Rhodamine B; MO = Methyl Orange; W represent watts.

2.8.2 Coupled Semiconductors

As tabulated in Table 2.2, formation of heterojunction with semiconductors of different energy levels is another widely used approach to improve the photocatalytic performance of BiOBr. Such process facilitates the inhibition of electron-hole recombination and depending on the coupled semiconductor, absorption wavelength might also be further extended into the higher visible region.

The bismuth-based semiconductors are among the most widely used coupling semiconductors to BiOBr. Qiu *et al.* (2017) loaded different amounts of bismuth subcarbonate ($\text{Bi}_2\text{O}_2\text{CO}_3$) onto BiOBr nanosheets. The absorption edge of the formed p-BiOBr/n- $\text{Bi}_2\text{O}_2\text{CO}_3$ composites exhibited a faint blue shift with further loading of n- $\text{Bi}_2\text{O}_2\text{CO}_3$. Therefore, the enhanced performance of the composites was attributed to the p-n heterojunction which facilitates charge separation and suppressed recombination, rather than increase in visible-light optical absorption (Qiu *et al.*, 2017).

In another study related to the formation of heterojunction with bismuth-based semiconductors, Su and Wu (2018c) constructed a phase heterojunction of BiOBr and $\text{Bi}_4\text{O}_5\text{Br}_2$ nanosheets. However, in this case, rather than loading different amounts of $\text{Bi}_4\text{O}_5\text{Br}_2$ onto BiOBr, the BiOBr/ $\text{Bi}_4\text{O}_5\text{Br}_2$ composites were synthesized at different pH values (4, 5, 6 and 7). It was observed that, the absorption edge of the composites exhibited a red shift with the increase in pH value. BiOBr/ $\text{Bi}_4\text{O}_5\text{Br}_2$ composite synthesized at pH 7 has the highest efficiency for the photocatalytic degradation of ciprofloxacin, far better than pristine BiOBr or pristine $\text{Bi}_4\text{O}_5\text{Br}_2$.

Another approach that is now gaining more attention, involves coupling BiOBr with metal-free carbonaceous materials such as graphene and carbon quantum dots (CQDs). The use of CQDs have been reported by Duo *et al.* (2016). In their work, different amounts of CQDs were loaded onto BiOBr, by simply varying the amount of CQDs solution, forming 1-CQDs/BiOBr, 3-CQDs/BiOBr and 6-CQDs/BiOBr composites. A red shift of absorption band edges was observed with further loading of CQDs onto BiOBr. Similarly, during application under 500 W Xe lamp as the light source, pristine BiOBr degraded only 67% of RhB in 20 min, while 3-CQDs/BiOBr degraded 92%. Furthermore, Xia *et al.* (2016a) also synthesized a series of CQDs/BiOBr composites by simply controlling the weight ratio of CQD to BiOBr. After 30 min of irradiation using 300 W Xe lamp, 3 wt% CQDs/BiOBr has completely degraded RhB dye, while pristine BiOBr degraded only 37%. Such results have shown that, loading an optimal amount of CQDs onto BiOBr would lead to enhanced photocatalytic performance, due to improved optical absorption and higher separation efficiency of photogenerated charge carriers.

Apart from the aim of improving optical absorption and suppressing electron-hole recombination, nowadays, formation of heterojunction with some coupling semiconductors also facilitates convenient separation of photocatalysts from contaminant solution after use. For example, Li *et al.* (2017e) synthesized a series of magnetically separable BiOBr/NiFe₂O₄ composites via hydrothermal method by simply varying the weight percent of NiFe₂O₄ introduced to produce pristine BiOBr, BiOBr/NiFe₂O₄-5%, BiOBr/NiFe₂O₄-10%, BiOBr/NiFe₂O₄-15%, BiOBr/NiFe₂O₄-20% and BiOBr/NiFe₂O₄-25%. Loading more NiFe₂O₄ onto BiOBr strengthened both the light absorption capacity

and Brunauer-Emmett-Teller (BET) specific surface area of the BiOBr/NiFe₂O₄ composites. In terms of application, BiOBr/NiFe₂O₄-20% displayed the best photocatalytic performance and was able to degrade 90% methylene blue dye within 60 min. The slight decrease noticed in the case of BiOBr/NiFe₂O₄-25% was attributed to the high amount of NiFe₂O₄ on BiOBr surface which might hinder light contact with BiOBr. During application, the use of BiOBr/NiFe₂O₄ composites was marked as a convenient process, due to their easy and recyclable magnetic separation.